



FIR-based symmetrical acoustic beamformer with a constant beamwidth



Oren Rosen*, Israel Cohen, David Malah (Member, EURASIP)

Department of Electrical Engineering, Technion - Israel Institute of Technology, Haifa 3200003, Israel

ARTICLE INFO

Article history:

Received 30 December 2015

Received in revised form

14 April 2016

Accepted 18 July 2016

Available online 21 July 2016

Keywords:

Constant beamwidth beamformers

FIR-based beamformers

Microphone arrays

Robust beamformers

ABSTRACT

Traditional beamformer design methods suffer from a frequency varying beamwidth, making them less effective for wideband applications. Existing approaches that try to solve this problem demonstrate degraded beamformer performance in terms of sidelobe level attenuation and sensitivity, making them less robust to interference and array attribute perturbations. Another common issue for existing approaches is high computational complexity, resulting in the ability to implement these approaches only for small microphone arrays, directly affecting the beamformer spatial resolution. In this paper, we introduce a new approach for designing a constant beamwidth beamformer. The proposed approach utilizes custom-tailored finite impulse response (FIR) filters for each microphone channel, manipulating the beampattern to achieve a desired beamwidth. The manipulated beampattern has approximately a constant beamwidth over a wide frequency band. Additionally, a post-summing output normalization filter is used to ensure a frequency invariant gain of the beampattern. By exploiting the physical microphone array configuration and attributes, we shape accordingly the frequency response of the FIR filters and control the beamformer beamwidth. The proposed approach demonstrates improved array response results in various scenarios, compared to available methods in the field, especially in terms of sensitivity to parameters mismatch, noise robustness and sidelobe attenuation.

© 2016 Elsevier B.V. All rights reserved.

1. Introduction

Array beamforming has been a significant research topic of signal processing and communication theory in the past three decades. Originally, it was dedicated to radar and sonar applications [1,2] and subsequently became an important research topic in the fields of seismology, medical diagnosis, communications, radio astronomy and many other fields [3–5] as well.

A beamformer with a fixed beamwidth over a wide frequency band is termed a constant beamformer. Constant beamwidth beamformer designs have been investigated mainly in the field of speech processing with microphone arrays, where various approaches have been proposed [6–14]. Traditional beamformer design approaches such as the Capon beamformer [15], the projection beamformer [16] and the blocking matrix beamformer [17] did not provide sufficient performance in terms of beamwidth constancy, sensitivity to parameters mismatch, and noise robustness. Therefore, numerous contemporary approaches to robust beamformer designs were proposed. The minimum variance distortionless response (MVDR) [18,19], linearly constrained minimum variance (LCMV) [20], least-squares [21,22],

hybrid steepest-descent [23], and eigenspace based beamformers [24] are several beamforming design techniques developed for improving the traditional methods.

One of the popular beamformer design approaches is the FIR based beamformer [25–29]. FIR beamformers perform temporal filtering that results in a frequency dependent response. The filtering is performed in order to compensate for the phase difference of various frequency components. It has been shown [30,31] that utilizing narrowband FIR filters in beamformer designs can produce robust beamformers. Nevertheless, the task of generating a constant beamwidth over a wide frequency band still remains a challenging problem.

In this paper, we propose a new approach for a constant beamwidth beamformer design. By utilizing FIR filter arrays and array symmetry attributes, we offer a microphone array design method that yields an array response characterized by an approximately constant beamwidth and improved robustness to parameters mismatch, compared to various other design methods, even in the case of microphone imperfections. The paper is organized as follows. In Section 2, we provide background material and formulate the problem. Section 3 describes the proposed beamformer design method. Section 4 describes the experimental setup and demonstrates the performance of the proposed algorithm. Finally, Section 5 concludes the paper.

* Corresponding author.

E-mail address: roseno@tx.technion.ac.il (O. Rosen).

2. Background and problem formulation

In this section, we provide background material on filter-based beamformer design and formulate the constant beamwidth problem. Microphone arrays are utilized for filtering signals in a space-time field. Filtering is enabled by exploitation of the incoming signals spatial characteristics and may be expressed in terms of angle and wave number dependency. A desirable spatial filtering, i.e., beamforming, should result in enhancement of signals of interest, originated in a specific direction, while forcing suppression of undesired signals originated in other directions. Many factors must be taken into consideration when designing a beamformer. First of all, the array geometry forces fundamental constraints on the beamformer's operation. In most cases, the array geometry is the first consideration in array design due to practical and physical constraints. Therefore, the degree of freedom in choosing the array geometry is limited. Secondly, the weights applied to array microphones determine the spatial filtering characteristics of the beamformer as well as the array performance in terms of measures like sensitivity and directivity.

2.1. Microphone array configuration

A conventional beamformer [32] is composed of a Uniform Linear Array (ULA) of microphones. That is, the microphones are positioned on an axis with a uniform spacing between the microphones. The general expression of the microphone positioning in a ULA is given by:

$$x_m = m \cdot d, \quad m = 0, 1, \dots, M - 1 \quad (1)$$

where m denotes the microphone index; x_m denotes the position of the microphone having index m , where $x_m=0$ corresponds to the left-hand side of the array, i.e., the location where the microphone indexed by $m=0$ is positioned; d denotes the spacing between microphones, and M is the array size, i.e., the number of microphones in the array, as demonstrated in Fig. 1(a) for the case of an even number of microphones and (b) for the case of an odd number of microphones. The center of the microphone array, i.e., the symmetry point, is set to be at $x = \left(\frac{M-1}{2}\right)d$.

The array microphones spatially sample the incoming signals, and processing them to attenuate signals from undesired directions and extract the signal from a desired direction. A spatial response of the microphone array is obtained via a beam (main

lobe) directed to the desired signal while nulls are directed to the undesired signals. Fig. 2 illustrates a beamformer design based on the linear array as shown in Fig. 1.

Let $\mathbf{f}(t, \mathbf{x})$ denote the set of signals sampled by the microphone array at time t , expressed by

$$\mathbf{f}(t, \mathbf{x}) = [f(t, x_0), \dots, f(t, x_{M-1})]^T, \quad (2)$$

where x_m denotes the microphone position, t denotes the continuous-time variable, and T denotes the transpose operation. The beamformer output $y(t)$ is given by:

$$y(t) = \sum_{m=0}^{M-1} f(t, x_m)w_m^*, \quad (3)$$

where w_m is a complex weight of the microphone having index m , as shown in Fig. 2, and $*$ denotes complex conjugation. The simplest beamformer design architecture has uniform weights, $w_m = \frac{1}{M}$, $m = 0, \dots, M - 1$.

Let $f_\omega(t) = e^{j\omega t}$ denote a plane wave propagating at angular frequency ω , and let $\theta \in \left[-\frac{\pi}{2}, \frac{\pi}{2}\right]$, denote the direction of arrival (DOA) angle measured with respect to the broadside of the linear array, as shown in Fig. 2. The wave signals spatially sampled by the microphone array inputs are given by:

$$\mathbf{f}_\omega(t, \mathbf{x}) = [f_\omega(t - \tau_0), \dots, f_\omega(t - \tau_{M-1})]^T, \quad \tau_m = \frac{\sin(\theta) \cdot x_m}{c}, \quad (4)$$

where τ_m is the propagation delay for the incoming signal and $c = 340 \text{ m s}^{-1}$ denotes the velocity of sound propagation in air. A value of $\tau_m = 0, \forall m$ implies a DOA of $\theta = 0$, i.e., a plane wave parallel to the array, propagating perpendicular to the array. Let $\kappa = \frac{\omega}{c} \sin(\theta) = \frac{2\pi}{\lambda} \sin(\theta)$ denote the wavenumber for plane waves in a locally homogeneous medium, where λ denotes the wavelength corresponding to the angular frequency ω , and let $\mathbf{v}(\kappa)$ denote the *array manifold vector* [32], featuring all of the spatial characteristics of the microphone array. Based on (4), and the definition of κ above, the manifold vector can be expressed as:

$$\mathbf{v}(\kappa) = [e^{-j\kappa x_0}, \dots, e^{-j\kappa x_{M-1}}]^T \quad (5)$$

Let $P(\omega, \theta)$ denote the frequency and DOA dependent beamformer response. It is given by:

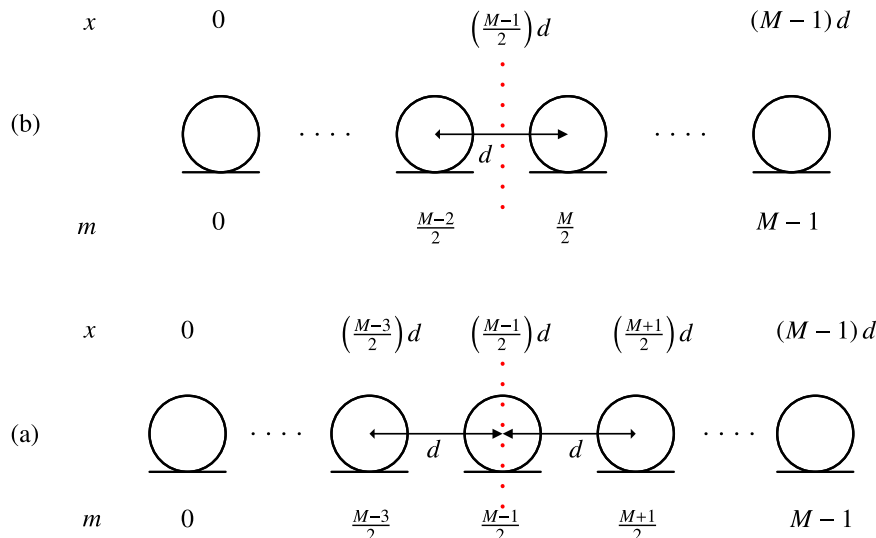


Fig. 1. A uniform linear array of size M : (a) M even and (b) M odd, with spacing d . The vertical dotted line denotes the symmetry point of the array located at $x = \left(\frac{M-1}{2}\right)d$.

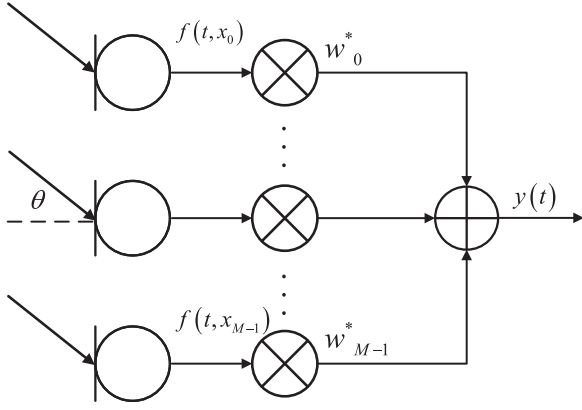


Fig. 2. A simple beamformer design.

$$P(\omega, \theta) = \sum_{m=0}^{M-1} e^{-j\omega\tau_m} w_m^* = \mathbf{w}^H \mathbf{v}(\omega, \theta), \quad (6)$$

where $\mathbf{w} = [w_0, \dots, w_{M-1}]^T$ and H denotes Hermitian transpose operation.

Beampatterns are the main tool in assessing an array performance as they express the beamformer response for various frequencies and signal angles. Let $D(\omega, \theta)$ denote the beampattern of a given beamformer. It is expressed by:

$$D(\omega, \theta) = 20 \log_{10} |P(\omega, \theta)|, \quad (7)$$

where $|\cdot|$ denotes the absolute value. For a given angular frequency ω , the beampattern $D(\omega, \theta)$ is a function of the angle θ and the beamwidth is measured in terms of θ . In this work, the beamwidth is measured between the two lowest values at both sides of the main lobe. So, when attainable, it is the *beamwidth null to null*, i.e., the width between zeroes of the main lobe [32], given by $2 \sin^{-1} \left(\frac{2\pi c}{Md\omega} \right)$.

The relation between the temporal frequency, $f = \frac{\omega}{2\pi}$, the number of microphones and the beamwidth, θ_{BW} can be obtained from the following expression:

$$\sin \left(\frac{\theta_{BW}}{2} \right) = \frac{2\pi c}{Md\omega} = \frac{c}{Mdf} \quad (8)$$

Thus, as the temporal frequency f increases, the beamwidth decreases.

2.2. Temporal filtering by an FIR filter array

Simple beamformers, as shown in Fig. 2., utilize a single weight for each microphone. This makes them ineffective when dealing with wideband signals, the signals of interest in speech and audio processing, as each of the signals is composed of various frequency components. In order to design a beamformer for wideband signals, the weight values in (6) must be altered for different frequencies in order to obtain the desired beamformer output. Thus, the weights should be frequency dependent, in the form of $\mathbf{w}(\omega) = [w_0(\omega), \dots, w_{M-1}(\omega)]^T$. This can be achieved by introducing discrete-time FIR filters [25,30].

FIR filters perform temporal filtering in order to compensate for the phase differences of the input wideband signals' various frequency components. Fig. 3. shows the realization of frequency dependent weights by FIR filters connected to the microphone array. Let $y(t)$ denote the output of the FIR-based beamformer. It is achieved by:

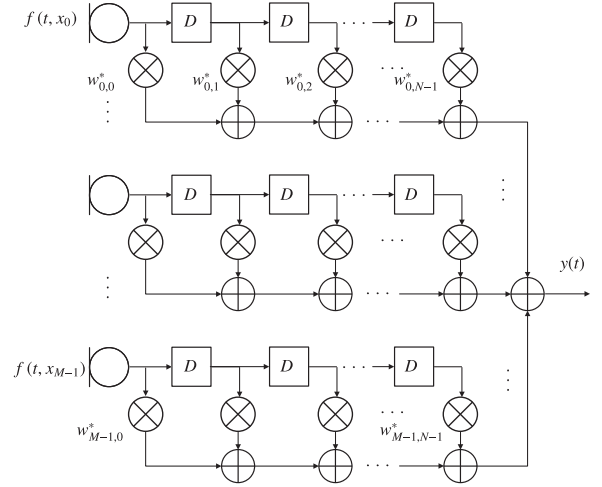


Fig. 3. FIR beamformer architecture, where D denotes a delay element.

$$y(t) = \sum_{m=0}^{M-1} \sum_{n=0}^{N-1} f(t - nT_s, x_m) \cdot w_{m,n}^* \quad (9)$$

where N denotes the number of FIR filter coefficients connected to each of the M microphones, $w_{m,n}^*$ is the n -th coefficient of the FIR filter connected to the microphone indexed by m , and T_s denotes the delay between adjacent filter elements. For an input complex plane wave signal, $e^{j\omega t}$, the beamformer output is given by:

$$y(t) = e^{j\omega t} P(\omega, \theta) = e^{j\omega t} \sum_{m=0}^{M-1} \sum_{n=0}^{N-1} e^{-j\omega(\tau_m + nT_s)} \cdot w_{m,n}^* \quad (10)$$

Let $\mathbf{v}_s(\omega, \theta)$ denote a *stacked array manifold vector* of dimension $M \cdot N$, where each subvector of dimension M represents the array manifold vector associated with a specific FIR filter coefficient in (10), i.e., the first subvector, $[e^{-j\omega\tau_0}, \dots, e^{-j\omega\tau_{M-1}}]^T$, is associated with the coefficient indexed by $n=0$ and all of the array microphones, indexed by $m = 0, \dots, M-1$. Thus, it is denoted by $\mathbf{v}_0(\omega, \theta)$. The second subvector, $[e^{-j\omega(\tau_0+T_s)}, \dots, e^{-j\omega(\tau_{M-1}+T_s)}]^T$, is associated with the coefficient indexed by $n=1$, and all of the array microphones. Thus, it is denoted by $\mathbf{v}_1(\omega, \theta)$, and so on. This form of expression is called *vector stacking*, and $\mathbf{v}_s(\omega, \theta)$ is given by:

$$\mathbf{v}_s(\omega, \theta) = \begin{bmatrix} \mathbf{v}_0(\omega, \theta) \\ \mathbf{v}_1(\omega, \theta) \\ \vdots \\ \mathbf{v}_{N-1}(\omega, \theta) \end{bmatrix}. \quad (11)$$

Given a ULA of M microphones, microphone spacing d , and M FIR filters, each composed of N coefficients, and connected to a respective microphone. Then, from (10) and (4), the beamformer response can be expressed as:

$$P(\omega, \theta) = \sum_{m=0}^{M-1} e^{-j\omega\tau_m} \sum_{n=0}^{N-1} e^{jn\omega T_s} \cdot w_{m,n}^* = \mathbf{w}_s^H \mathbf{v}_s(\omega, \theta), \quad (12)$$

where \mathbf{w}_s denotes the composite stacked weight vector of dimension $M \cdot N$ created by vector stacking, having $\mathbf{w}_0 = [w_{0,0}, w_{0,1}, \dots, w_{0,N-1}]^T$ as its first subvector, $\mathbf{w}_1 = [w_{1,0}, w_{1,1}, \dots, w_{1,N-1}]^T$ as its second subvector, and so on. The design specification of the FIR filters will be addressed in Section 3.

The second summation in (12) can be expressed in terms of the Discrete-time Fourier transform (DTFT) of the m -th channel filter coefficients as follows:

$$\sum_{n=0}^{N-1} e^{jn\omega T_s} w_{m,n}^* = W_m^*(e^{j\omega T_s}), \quad (13)$$

where $W_m(e^{j\omega T_s})$ denotes the DTFT of $w_{m,n}$ with the summation variable n . Hence, the expression for $P(\omega, \theta)$ in (12) can be written as:

$$P(\omega, \theta) = \sum_{m=0}^{M-1} e^{-j\omega \tau_m} W_m^*(e^{j\omega T_s}). \quad (14)$$

Since the channel filters have each a finite number of coefficients (N), their frequency responses can be represented by the Discrete Fourier transform (DFT) of size N of each filter coefficient. This corresponds to sampling ω at $\frac{2\pi}{NT_s}k$, $k = 0, \dots, N-1$. Examining the beamformer response for frequencies corresponding to the bin centers defined by the DFT, we obtain:

$$P(k, \theta) = \sum_{m=0}^{M-1} e^{-j\frac{2\pi\tau_m k}{NT_s}} W_m^*(e^{j\frac{2\pi k}{N}}), \quad k = 0, \dots, N-1, \quad (15)$$

where k denotes the bin index of the DFT. This expression will be the basis for controlling the beamformer frequency response by specifying the frequency response of the FIR channel filters.

Many methods have been proposed for determining the FIR filter coefficients. The main goal of these methods is obtaining a desirable beamformer output while dealing with trade-offs between conflicting array performance measures. Traditionally, the performance measures of interest are the main lobe response, sidelobe levels, sensitivity to parameters mismatch, robustness to noise, directivity and aliasing. Frequency dilation based FIR beamformers [31] derive the FIR filter coefficients from a single reference frequency response, thus deriving all of the filter coefficients, which are microphone location dependent, from a single set of coefficients. This results in a constant beamwidth approximation in a wideband on one hand, but also in high sidelobe levels and low robustness on the other hand. Optimization-based beamformer designs such as the MVDR and LCMV beamformers [18,20] force specific constraints on the beamformer weights and output. Therefore, these methods are chosen when a specific beamformer performance measure is needed to be optimized. Optimization-based methods often suffer from high computational complexity, resulting in the ability to implement these approaches only for small microphone arrays, directly affecting the beamformer spatial resolution. The following Section elaborates on the proposed method for determining the FIR filter coefficients that result in an approximate constant beamwidth beamformer for a wide range of input frequencies. Although the proposed method yields inferior beamwidth constancy in the lower frequency range than some methods, it offers improved array performance in terms of sidelobe attenuation, sensitivity and robustness, as well as a simple design method which is closed form.

3. Proposed FIR design algorithm

In this section, we present the proposed FIR design method that aims to obtain a constant beamwidth beamformer while maintaining lower levels of sidelobes compared to traditional methods [31]. The main feature of the proposed method is the determination of the FIR filter coefficients that provide a good approximation to a desired beamformer response. We consider real FIR coefficients since the signals of interest, i.e., acoustic signals, are real. For this purpose, we need first to determine the *minimal frequency*, i.e., the lowest frequency for which the desired beamwidth is feasible, given the array configuration. Then, the frequency response of each of the FIR filters is specified. To maintain a fixed delay by all the filters, they are designed to have a

linear phase and use each the same number of coefficients. Finally, a post-summing FIR normalization filter is introduced at the output of the array to maintain a uniform gain of the beam at all the frequencies for which it is designed to have a constant beamwidth.

3.1. Frequency range determination for constant beamwidth realization

The beamwidth of a given array is generally frequency dependent and gets smaller as the frequency increases. Thus, for a given desired beamwidth θ_{BW} , and a given array of size M , there exists a *minimal frequency*, denoted f_0 , for which θ_{BW} is realized. It is given that from (8) by:

$$f_0 = \frac{c}{Md \sin\left(\frac{\theta_{BW}}{2}\right)}, \quad (16)$$

where the desired beamwidth, i.e., the main lobe, extends from $-\frac{\theta_{BW}}{2}$ to $\frac{\theta_{BW}}{2}$. Hence, for input frequencies below f_0 the given array will produce a wider beamwidth than desired. Moreover, at higher frequencies than f_0 , a lower beamwidth will be realized if no FIR filters are added.

To keep a constant beamwidth of θ_{BW} , as the frequency of the impinging wave increases, we need to keep the product Mf constant. Since only a single frequency satisfies a constant Mf for a given M , M must be changed to satisfy this relation for various f values. We designate the microphones that satisfy a constant Mf as *effective microphones*. That is, as the wave frequency increases, the effective number of participating microphones in the array, denoted by M_p , is reduced by means of signal attenuation by the appropriate FIR filters. Since M_p must be an integer, the product constancy will be satisfied exactly only for a set of frequencies, while between those frequencies it is approximately satisfied.

For a given array size, M , M_p is limited to the range: $M_{\min} \leq M_p \leq M$, $M_p = M - 2p$, $p = 1, 2, \dots, \frac{M-M_{\min}}{2}$. Theoretically, $M_{\min} = 1$, but this value is not feasible since a single microphone is necessarily omni-directional and therefore cannot produce the desired beamwidth, assuming $\theta_{BW} < 2\pi$. Thus, the minimal value of M_p is $M_{\min} = 3$, for an odd number of microphones (M odd), and $M_{\min} = 2$ for an even number of microphones (M even), maintaining symmetry around $x = (\frac{M-1}{2})d$. Substituting the value of M_{\min} in (16) we obtain the maximal frequency, denoted f_{\max} , for which we can still maintain the fixed beamwidth. For frequencies beyond f_{\max} the beam will be narrower than desired. Thus, the proposed approach can provide an approximate constant beamwidth in the range $[f_0, f_{\max}]$.

Different applications may desire a narrower range of frequencies for which the beamwidth is constant, say $[f_L, f_H]$, $f_0 \leq f_L < f_H \leq f_{\max}$, allowing a reduced complexity array, as will be discussed in Sections 3.2.1 and 3.4.

We continue here with the maximal range, i.e., $f_L = f_0$ and $f_H = f_{\max}$. As the frequency increases within that range, the number of effective microphones needs to be reduced. This can be done only in decrement steps of 2, i.e., $M_1 = M - 2$, $M_2 = M - 4$, and so on, maintaining symmetry by effectively removing at each step one microphone from each end of the array and calculating a corresponding minimal frequency f_p , $f_L < f_p \leq f_H$, by replacing M by M_p in (16). Note that because M_p varies in decrements of 2 and not continuously, the beamwidth will fluctuate for frequencies between adjacent f_p values. This issue will be demonstrated and alleviated in the sequel.

3.2. FIR filter design

Consider a symmetric ULA and let $P(f, \theta)$, denote its beamforming response. The proposed algorithm plugs in an FIR filter at each microphone input line, as in Fig. 3. Each FIR filter is of length

N and can be represented by its frequency response, calculated by applying a length N DFT to the filters coefficients. This results in N frequency coefficients, one per each of the N frequency bins in $[0, \frac{1}{T_s})$, where T_s is the sampling interval of the input signal, i.e., the temporal sampling period of the system. The rationale behind the selection of T_s is discussed in Section 3.2.1. The design algorithm specifies custom frequency response coefficients of each filter needed to obtain a constant beamwidth beamformer.

3.2.1. Basic design

The proposed approach for maintaining an approximate fixed beamwidth in the specified frequency range is to reduce the number of effective microphones by attenuating the signal from specific microphones as the frequency increases. This is achieved by letting the real FIR filters to be lowpass filters with cutoff frequencies set according to the values of $f_p, p = 1, 2, \dots, \frac{M-M_{\min}}{2}$, as shown in Fig. 4, for M odd.

The expression in (15) gives the beamformer frequency response at N discrete frequencies in terms of the DFT of the FIR filters coefficients. Let \mathbf{W} denote an $N \times M$ matrix denoted the filter array matrix based on this expression. The matrix is composed of m columns, $m = 0, 1, 2, \dots, M - 1$, where each column element is given by $W_{in}(e^{j\frac{2\pi}{N}k})$, corresponding to the DFT of the m -

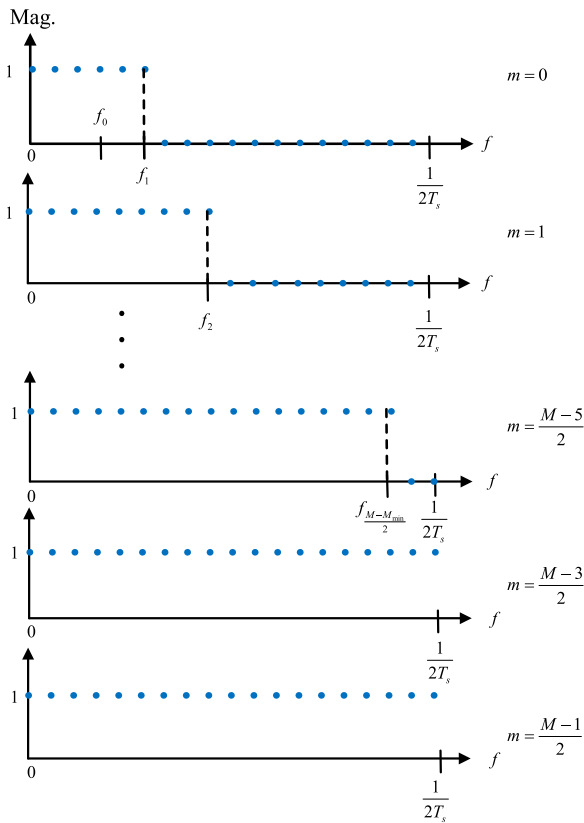


Fig. 4. The desired frequency responses of the FIR filters for the lower half of the frequency range, indexed by microphone index $m = 0, \dots, \frac{M-1}{2}, M$ odd. Due to the microphone array symmetry, the magnitude response specification for the filters connected to the second half of the array, i.e., for $m = \frac{M+1}{2}, \dots, M - 1$, is a mirror image of first half of the array. Each dot in the specified response is the value of the filter magnitude at a corresponding frequency bin. Since M is odd and due to symmetry, the two bottom rows of Fig. 4 represent all-pass FIR filters since $M_{\min} = 3$. This means that three microphones are effective at all frequencies. For M even, only two microphones would be effective at all frequencies since $M_{\min} = 2$ and therefore only the FIR filter connected to the microphone indexed by $m = \frac{M-1}{2}$, i.e., the last row, would be an all-pass filter.

th channel filter coefficients. For the sake of simplified notation, and because the magnitude response of a causal linear-phase filter is the same as that of a zero-phase filter, we continue here with a zero phase filter. Since the magnitude responses of the considered filters have mirror-image symmetry with respect to half the sampling frequency, we partition \mathbf{W} into two blocks:

$$\mathbf{W} = \begin{bmatrix} \mathbf{W}_L \\ \mathbf{W}_H \end{bmatrix}, \quad (17)$$

where both \mathbf{W}_L and \mathbf{W}_H are of size $L \times M$, and L is the number of frequency bins in the lower band, i.e., up to half the sampling frequency, such that the columns of \mathbf{W}_L represent the magnitude response of the filters in the lower band, i.e., up to half the sampling frequency, and the columns of \mathbf{W}_H represent those of the upper band, up to the sampling frequency. Hence, we refer only to \mathbf{W}_L in the following design process.

For an odd number of microphones (M odd), \mathbf{W}_L is specified as:

$$\mathbf{W}_L = \begin{matrix} m = 0 & m = \frac{M-1}{2} & m = M-1 \\ \begin{pmatrix} 1 & 1 & 1 & 1 & \dots & 1 & 1 & 1 & \dots & 1 & 1 & 1 & 1 \\ \vdots & & & & & \vdots & & & & \vdots & & & \\ 1 & 1 & 1 & 1 & \dots & 1 & 1 & 1 & \dots & 1 & 1 & 1 & 1 \\ 1 & 1 & 1 & 1 & \dots & 1 & 1 & 1 & \dots & 1 & 1 & 1 & 1 \\ \vdots & & & & & \vdots & & & & \vdots & & & \\ 1 & 1 & 1 & 1 & \dots & 1 & 1 & 1 & \dots & 1 & 1 & 1 & 1 \\ 0 & 1 & 1 & 1 & \dots & 1 & 1 & 1 & \dots & 1 & 1 & 1 & 0 \\ \vdots & & & & & \vdots & & & & \vdots & & & \\ 0 & 1 & 1 & 1 & \dots & 1 & 1 & 1 & \dots & 1 & 1 & 1 & 0 \\ 0 & 0 & 1 & 1 & \dots & 1 & 1 & 1 & \dots & 1 & 1 & 0 & 0 \\ \vdots & & & & & \vdots & & & & \vdots & & & \\ 0 & \dots & \dots & \dots & 0 & 1 & 1 & 1 & 0 & \dots & \dots & \dots & 0 \end{pmatrix} & \begin{matrix} f = 0 \\ \vdots \\ f = f_0 \\ \vdots \\ f = f_1 \\ \vdots \\ f = f_2 \\ \vdots \end{matrix} \end{matrix} \quad (18)$$

The columns of \mathbf{W}_L are the magnitude specifications of the FIR channel filters, as shown in Fig. 4. The row indices of \mathbf{W}_L correspond to the bin frequencies in the lower band. That is, the first row of \mathbf{W}_L in (18), corresponds to the frequency bin centered at $f=0$, and the last row corresponds to half the sampling frequency. Since M is odd in (18), the 3 central columns of \mathbf{W}_L , corresponding to $M_{\min} = 3$, are specified as all 1's, i.e., allpass filters. For an even number of microphones M , the matrix in (18) would contain 2 central columns with all 1's, corresponding to $M_{\min} = 2$.

The first column of \mathbf{W}_L is the magnitude response of the FIR filter indexed by $m = 0$. The row corresponding to frequency f_1 , indicates the cutoff frequency of that filter. For frequencies from f_1 up to f_2 , $M_1 = M - 2$ microphones are effective. For the range $[0, f_1)$ all the M microphones are effective. The second column of \mathbf{W}_L is the magnitude response of the FIR filter indexed by $m=1$. Similarly, the frequency f_2 indicates the cutoff frequency of the filter associated with the second column. For frequencies from f_2 up to f_3 (not shown in (18)), $M_2 = M - 4$ microphones are effective, and so on. The number of effective microphones may reach $M_{\min} = 3$ at a lower frequency than half the sampling frequency, unless $f_{\max} = \frac{1}{2T_s}$. If $f_H < f_{\max}$, the number of effective microphones need not reach M_{\min} but would be higher (matching f_H), so more columns in \mathbf{W}_L should be set all 1's, i.e., all-pass filters. A similar situation will occur if the sampling frequency is set so that $\frac{1}{2T_s} < f_{\max}$, since f_H must then be set to half the sampling frequency, i.e., $\frac{1}{2T_s}$.

In reality, a causal filter is eventually implemented by shifting the filter coefficients, resulting in a linear-phase causal filter with the same magnitude response. The basic design above improves the beamformer response, compared to the conventional one, in terms of beamwidth constancy, as demonstrated in Fig. 5(a) and (b). Yet, because M_p varies in steps of 2, the beamwidth does vary at frequencies that are between adjacent cutoff frequencies, causing fluctuations in the beamwidth, as clearly seen in Fig. 5(b). To reduce these fluctuations in beamwidth a modified design is proposed next.

Note also that for frequencies in between adjacent bins, the frequency response of the FIR filters also diverts from the desired ideal low-pass response because of the finite number of filter coefficients (N). By increasing N , the latter effect is reduced but at the expense of increased computational complexity.

3.2.2. Modified design

The beamwidth fluctuations noted above can be alleviated by modifying the specifications of some of the FIR filters in the array to include intermediate magnitude values, denoted as *smoothing magnitude coefficients*, in the transition band between the cutoff frequency of those filters to the cutoff frequency of the next filter in the array, as shown in Fig. 6. The corresponding form of the modified FIR magnitude response matrix \mathbf{W}_L is shown in (19). As in Section 3.2.1, we initially design a zero-phase FIR filter and eventually implement a causal filter by shifting the filter coefficients, resulting in a linear-phase causal filter with the same magnitude response. Let k denote the index corresponding to the k -th bin frequency. A row of \mathbf{W}_L consists of the responses of all the array filters at a given bin frequency, e.g., the row of \mathbf{W}_L corresponding to the frequency of f_0 , is given the frequency bin index k_0 . Due to the microphone array symmetry attributes, we define pairs of smoothing magnitude coefficients where every pair of coefficients is placed at symmetrical microphone indices, i.e., at $m = 0, M - 1$, for frequency bins indexed by $k_0 > k \geq k_2$; $m = 1, M - 2$, for frequency bins indexed by $k_2 > k \geq k_3$, and so on. Although M effective microphones should be used in the transition band $k_0 > k \geq k_1$ and $M - 2$ effective microphones should be used in

the transition band $k_1 > k \geq k_2$, we use $M - 2$ effective microphones for all bins in $k_0 > k \geq k_2$ to achieve the desired beamwidth. Utilizing M effective microphones in $k_0 > k \geq k_1$ would prevent controlling the beamwidth since there is no degree of freedom to widen the narrowing beamwidth in that range. We show below that these coefficients help in reducing the beamwidth fluctuations by adding a degree of freedom in controlling the beamwidth at those frequency bins that are between adjacent cutoff frequencies. Let $W_{k,m}$ denote the smoothing magnitude coefficients that are shown in Fig. 6.

As depicted in Fig. 6, \mathbf{W}_L takes the form shown in the following equation:

$$\mathbf{W}_L = \begin{pmatrix} 1 & 1 & \dots & 1 & 1 & \dots & 1 & 1 \\ \vdots & \vdots & & \vdots & \vdots & & \vdots & \vdots \\ 1 & 1 & \dots & 1 & 1 & \dots & 1 & 1 \\ W_{k_0+1,0} & 1 & \dots & 1 & 1 & \dots & 1 & W_{k_0+1,M-1} \\ W_{k_0+2,0} & 1 & \dots & 1 & 1 & \dots & 1 & W_{k_0+2,M-1} \\ \vdots & \vdots & & \vdots & \vdots & & \vdots & \vdots \\ W_{k_2-1,0} & 1 & \dots & 1 & 1 & \dots & 1 & W_{k_2-1,M-1} \\ 0 & W_{k_2,1} & 1 \dots & 1 & 1 & \dots & 1 & 0 \\ \vdots & \vdots & & \vdots & \vdots & & \vdots & \vdots \\ 0 & \dots & 0 & W_{\lfloor \frac{N}{2} \rfloor, \frac{m}{2}} & 1 & 1 & 1 & W_{\lfloor \frac{N}{2} \rfloor, \frac{(M-m)}{2}-1} & 0 \dots & 0 \end{pmatrix}$$

$k = k_0$

$k = k_2$

(19)

Because the array is symmetric, the pair of smoothing coefficients in the relevant rows, i.e., rows corresponding to $k > k_0$, is set

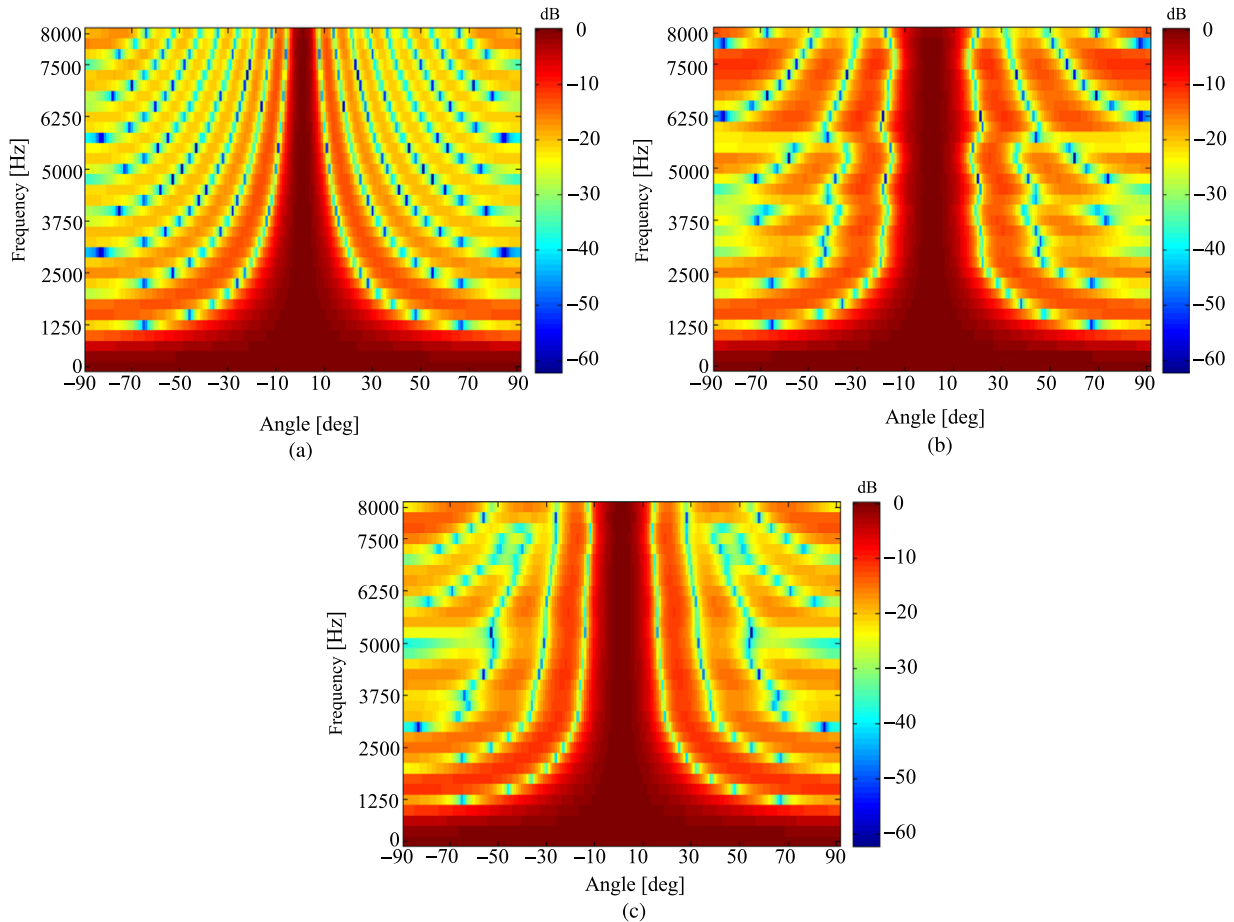


Fig. 5. Array beampattern of (a) a conventional array without FIR filters, (b) an FIR array with magnitude response \mathbf{W}_L , as given in (18), and (c) the modified design presented in the next section. The frequency range of $[0, \frac{1}{25}] = [0, 8]$ kHz is represented by the Y-axis and is quantized into $N=32$ frequency bins. The DOA range of $\theta = [-90, 90]^\circ$ is represented by the X-axis. For display purposes, the frequency response at a higher resolution is computed from the FIR filter coefficients. The desired beamwidth is $\theta_{BW} = 30^\circ$ and the minimal frequency is $f_0 = 3412$ Hz.

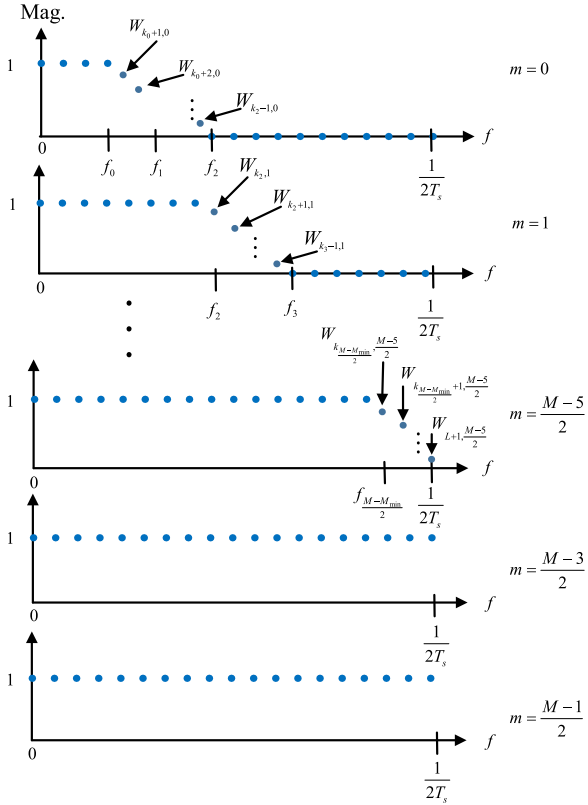


Fig. 6. Modified FIR magnitude responses for M odd, where $W_{k,m}$ denotes the FIR filter magnitude response at the frequency bin indexed by k and the microphone indexed by m .

to have equal values. Furthermore, to allow a closed form solution for these coefficients, at most one pair of such coefficients appears in each row. The smoothing coefficients values are then derived as follows.

Let f_k denote the k -th frequency bin, where $k = 0, \dots, L - 1$. The beamformer response at f_k , with the modified FIR filter array, is given, from (15) by:

$$P(f_k, \theta) = \frac{1}{M_p + 2W_{k, \lfloor \frac{M-M_p}{2} \rfloor - 1} \left(\sum_{m=\lfloor \frac{M-M_p}{2} \rfloor}^{M-\lfloor \frac{M-M_p}{2} \rfloor - 1} \left(e^{-j\frac{2\pi f_k}{c} m d \sin(\theta)} \right) + W_{k, \lfloor \frac{M-M_p}{2} \rfloor - 1} \cdot e^{j\frac{2\pi f_k}{c} \left(\lfloor \frac{M-M_p}{2} \rfloor - 1 \right) d \sin(\theta)} + W_{k, M-\lfloor \frac{M-M_p}{2} \rfloor} \cdot e^{-j\frac{2\pi f_k}{c} \left(M-\lfloor \frac{M-M_p}{2} \rfloor \right) d \sin(\theta)} \right)}$$

(20)

where $W_{k, \lfloor \frac{M-M_p}{2} \rfloor - 1}$ and $W_{k, M-\lfloor \frac{M-M_p}{2} \rfloor}$ denote the real smoothing magnitude coefficients at the k -th frequency bin of the filter, k_p denotes the k -th frequency bin corresponding to f_p , and $\frac{\sin(\theta) \cdot m \cdot d}{c}$ is substituted for τ_m in (15).

As stated above, the two unknown coefficients in (20) are set to have the same value, so that the unknown coefficient value can be found by forcing the beampattern to have a null at $\theta_{null} = \pm \frac{\theta_{BW}}{2}$.

Thus, we can find the smoothing magnitude coefficient $W_{k, \lfloor \frac{M-M_p}{2} \rfloor - 1}$ by setting $P(f_k, \theta_{null}) = 0$.

Since $\frac{1}{M_p + 2W_{k, \lfloor \frac{M-M_p}{2} \rfloor - 1}} \neq 0$, we get:

$$\sum_{m=\lfloor \frac{M-M_p}{2} \rfloor}^{M-\lfloor \frac{M-M_p}{2} \rfloor - 1} e^{j\frac{2\pi f_k}{c} m d \sin(\theta_{null})} = -W_{k, \lfloor \frac{M-M_p}{2} \rfloor - 1} \left(e^{-j\frac{2\pi f_k}{c} \left(\lfloor \frac{M-M_p}{2} \rfloor - 1 \right) d \sin(\theta_{null})} + e^{j\frac{2\pi f_k}{c} \left(\lfloor \frac{M-M_p}{2} \rfloor - 1 \right) d \sin(\theta_{null})} \right)$$

Using Euler and other trigonometric identities, we get:

$$\sum_{m=0}^{\lfloor \frac{M_p-1}{2} \rfloor} 2 \cos\left(\frac{2\pi f_k}{c} m d \sin(\theta_{null})\right) = -W_{k, \lfloor \frac{M-M_p}{2} \rfloor - 1} \left(2 \cos\left(\frac{2\pi f_k}{c} \left(\lfloor \frac{M-M_p}{2} \rfloor - 1 \right) d \sin(\theta_{null})\right) \right)$$

The final expression of the smoothing magnitude coefficient $W_{k, \lfloor \frac{M-M_p}{2} \rfloor - 1}$ is finally given by:

$$W_{k, \lfloor \frac{M-M_p}{2} \rfloor - 1} = -\frac{\sum_{m=0}^{\lfloor \frac{M_p-1}{2} \rfloor} \cos\left(\frac{2\pi f_k}{c} m d \sin(\theta_{null})\right)}{\cos\left(\frac{2\pi f_k}{c} \left(\lfloor \frac{M-M_p}{2} \rfloor - 1 \right) d \sin(\theta_{null})\right)}$$

(21)

Following the construction of \mathbf{W}_L in (19) and the placement of the new magnitude response coefficients calculated by (21), the discrete-time filter coefficients of each FIR filter are calculated by applying the IDFT to the corresponding column of \mathbf{W} . The construction of \mathbf{W} requires the construction of \mathbf{W}_H from \mathbf{W}_L based on the mirror image symmetry of the magnitude response of \mathbf{W}_L . Fig. 5(c) demonstrates the effect of the modification introduced in this section. It is clearly seen that the proposed modification results in a better approximation of a constant beamwidth beamformer, compared to the results shown in Fig. 5(a) and (b).

3.3. Post-summing FIR filter design

Following the input FIR filter array, an additional normalization FIR filter is added. It is needed to achieve a uniform gain at all the frequencies in the range $[f_L, f_H]$, as the frequency responses of the different FIR filters are not all the same. It is inserted at the beamformer output.

Let $\tilde{w}_k, k = 0, \dots, N - 1$, denote the samples of the normalization filter frequency response at N discrete frequencies, i.e., the DFT coefficients of the post-summing normalization FIR filter. The k -th DFT coefficient is set to:

$$\tilde{w}_k = \frac{1}{\sum_{m=0}^{M-1} |W_{k,m}|}$$

(22)

where $W_{k,m}$ denotes the coefficient of \mathbf{W}_L in (19) at the k -th row (frequency bin) and at the column indexed by m (the microphone index). For every frequency bin, the normalization filter sums the absolute values of the frequency response coefficients for the microphone filters from $m=0$ to $m = M - 1$. To achieve a uniform gain also at frequencies that are in between the N bin frequencies, more than N coefficients for the normalization filter are needed. The additional coefficients values can be computed by first obtaining a higher resolution frequency response of the FIR filters by zeros padding, as mentioned earlier, and then applying

normalization as in (22) for the additional frequencies. The normalization filter coefficients are then obtained by applying the IDFT to the frequency response coefficients. Fig. 7 illustrates the proposed complete FIR filter based beamformer structure.

3.4. Comments

If it is desired that the microphone array should not pass signal frequencies below f_0 , because the beamwidth at those frequencies is wider than desired, one can use FIR filters of the bandpass type, having their lower cutoff frequency at f_0 . However, bandpass filters are generally more complex to implement, therefore, the lowpass type would be usually preferred. Note that the bandpass filters could be designed to attenuate also signal frequencies above f_{\max} , if it is below $\frac{1}{2f_s}$.

In the design presented above we assumed that $[f_L, f_H] = [f_0, f_{\max}]$. However, if $f_L > f_0$, one can use less microphones in the array so as to match f_0 to the desired f_L .

The main disadvantage of the proposed method is the lack of control over the beamformer performance other than the beamwidth. The reviewed methods, which the proposed method was compared to, are based on optimization algorithms, enabling the introduction of constraints on various beamformer performances. The method proposed in [33], finds a maximum directivity beamformer and the algorithm proposed in [20] minimizes the side-lobe levels on top of achieving a constant beamwidth beamformer. Therefore, the proposed method should be less effective for scenarios where multiple beamformer constraints must be fulfilled.

Expression (16) is used for calculating the minimal frequency for which the desired beamwidth can be achieved. Since the proposed method assumes ULA geometry, only M varies in (16) for every decrement in the number of effective microphones. For other geometries, such as non-uniformly distributed linear arrays or UCA, it would be required to find a new expression for the minimal frequency in every microphone decrement step.

The limitation of the proposed method is that the minimal frequency calculation in (16) is valid only to ULA beamformers. The proposed method would be valid for other cases if an expression for the minimal frequency based on the array configuration could be calculated.

The proposed algorithm's main stages of array configuration and FIR filter design are summarized in Table 1.

4. Experimental results

In this section, we demonstrate the performance and advantages of the proposed algorithm via several experiments. We compare the acquired results to three different beamforming algorithms: (i) Parra's algorithm [26], where a least-squares optimal basis transform is calculated, decoupling the frequency response from the spatial response. (ii) The algorithm by Tourbabin et al. [33], where a real-valued solution to the maximum directivity optimization problem is presented. (iii) Doblinger's algorithm [20], where second-order cone programming based optimization is used together with sensor calibration. All of the simulated microphone arrays are configured with $M=11$ omnidirectional microphones. Moreover, each input channel is connected to a $N=32$ coefficient long FIR filter and the sampling frequency of the system is $f_s = 16$ kHz, where $f_s = \frac{1}{T_s}$. In Section 4.1 we run simulations for a uniform linear array with $d = 3.5$ cm spacing. Section 4.2 provides simulation results when microphone gain imperfection is induced by a random signal amplitude difference of up to 15% between the microphones. In Section 4.3 we provide simulation

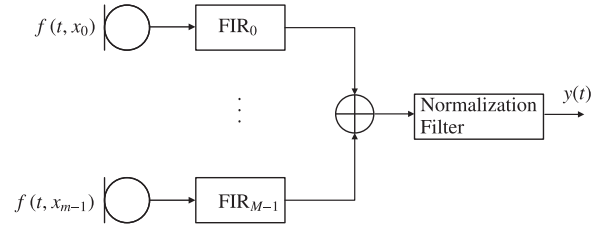


Fig. 7. Proposed FIR-based beamformer structure.

results for microphone array spacings perturbations induced by a random microphone positioning error of up to 10% from the nominal microphone positionings.

4.1. ULA experiments

In this section, the spacing between each of the $M=11$ microphones is $d = 3.5$ cm, the desired beamwidth is 30° , the frequency range is $[f_L, f_H] = [f_0, \frac{1}{2T_s}] = [3400, 8000]$ Hz. The simulation results are shown in Fig. 8 where the null-to-null beamwidth is bounded by the two black arrows in Fig. 8(a), the sidelobes are marked by the two white arrows in Fig. 8(b) and the aliasing phenomena are marked by the two gray arrows in Fig. 8(c). The examined algorithms run-times were 1.7 s, 2.6 s, 1.4 s and 37.1 s for the proposed, Parra's, Tourbabin's and Doblinger's methods, respectively. All simulations were ran on an Intel® core™ i5 2400 MHz with 4 GB RAM and Mathworks Matlab® R2012a. The proposed method run-time is comparable to the algorithm proposed by Tourbabin and Parra and superior to the run-time of Doblinger's algorithm.

In the following sub-sections, we elaborate on the performance of the various methods in beamwidth constancy, sidelobe attenuation, aliasing effects attenuation, sensitivity, microphone gain imperfections and array spacings perturbations.

4.1.1. Beamwidth

In Fig. 9 the effective beamwidths of the various methods are compared. The beamwidths are compared by their error relatively to the desired beamwidth $\theta_{BW} = 2\theta_{null}$, i.e., the difference between the null-to-null beamwidth of each algorithm and the desired beamwidth in the wideband.

The beamwidth constancy can be measured by the mean absolute error (MAE) between the beamwidth received by the various methods and the desired beamwidth in the examined frequency range. The received MAE values were 1.7° , 1.7° , 7.7° , 1.4° and 10° for the proposed, Parra's, Tourbabin's, Doblinger's and ULA

Table 1

Proposed FIR based constant beamwidth beamformer algorithm.

Array configurations:

1. Calculate the minimal and maximal frequency values f_0 and f_{\max} given the array specifications (number of array microphones M , desired beamwidth θ_{null} and spacing d) using (16).
2. Calculate $f_p, f_L < f_p \leq f_H$, by replacing M by M_p in (16).
 $M_{\min} \leq M_p \leq M - 2, p = 1, 2, \dots, (M - M_{\min})/2$.

Input FIR filters:

3. Construct the matrix \mathbf{W}_L as in (19).
4. Construct the matrix \mathbf{W}_H on the basis of the mirror image property of \mathbf{W} .
5. Construct the matrix \mathbf{W} by concatenating \mathbf{W}_L and \mathbf{W}_H .
6. Calculate the smoothing magnitude coefficients $W_k \left| \frac{M-M_p}{2} \right|_{-1}$ using (21); $k = 0, \dots, L - 1$.

Post-summing FIR filter:

7. Calculate the post-summing FIR filter coefficients using (22).

delay and sum methods, respectively. The reason for the somewhat inferior results of the proposed method, in comparison to two of the examined methods, is that these methods use optimization. However, the other methods do not offer direct control over the desired beamwidth as in the proposed method and have a more complex design algorithm because of optimization. The proposed method also offers better sidelobe attenuation and aliasing attenuation, as well as more robust performance when microphone gain imperfections and array spacings perturbations are introduced, as shown in the next sub-sections.

4.1.2. Sidelobe attenuation and output gain

To compare the sidelobe attenuation performance, Fig. 10 presents the beampatterns obtained for the different methods. The curves shown in Fig. 10 represent the beampatterns at different frequencies in the frequency range of [3400, 8000]Hz with increments of 230 Hz. The proposed algorithm demonstrates better sidelobe attenuation without compromising main-lobe beamwidth and output gain. The sidelobe levels are marked by the red dashed lines. A sidelobe attenuation of 13.42 dB is obtained for the proposed algorithm in Fig. 10(a), while sidelobe attenuations of 7.71 dB, 10.78 dB, and 14.72 dB are obtained for the other algorithms, as seen in Fig. 10(b), (c), and (d), respectively. The primary reason for the better sidelobe attenuation performance in the proposed algorithm is the explicit calculation of the beamwidth for every frequency bin, shown in (18)–(21), together with the

attenuation caused by the decreasing number of effective microphones, causing most of the power to stay within the main-lobe and not leak to the sidelobes. The algorithm proposed by Doblinger [20] minimizes the sidelobe levels at the expense of the main-lobe level, which is lower than 0 dB some frequencies, as shown in Fig. 10(d). The other methods do not take sidelobe levels attenuation performance into consideration. In Tourbabin's algorithm [33], lowering the sidelobe levels by using different cost functions decreases the performance of the algorithm's main objective.

In Fig. 10(a) and (c) the beampatterns have a uniform gain due to normalization factors. The proposed algorithm utilizes an output FIR post-summing normalization filter and Tourbabin's algorithm utilizes normalization constants for obtaining a uniform gain beampattern. Parra's and Doblinger's algorithms in Fig 9 (b) and (d) do not use normalizations factors and therefore yield non-uniform gain beampatterns. In Parra's algorithm, this phenomenon is more prevalent at low frequencies, while in Doblinger's algorithm it is more noticeable at higher frequencies. Output FIR normalization filters have been utilized as part of the FIR filter design in several beamforming design methods [6,31].

4.1.3. Aliasing attenuation

Spatial aliasing occurs when the array microphones sample the impinging signals from different locations not densely enough, i.e., the microphone spacing d is too large. This causes sources at

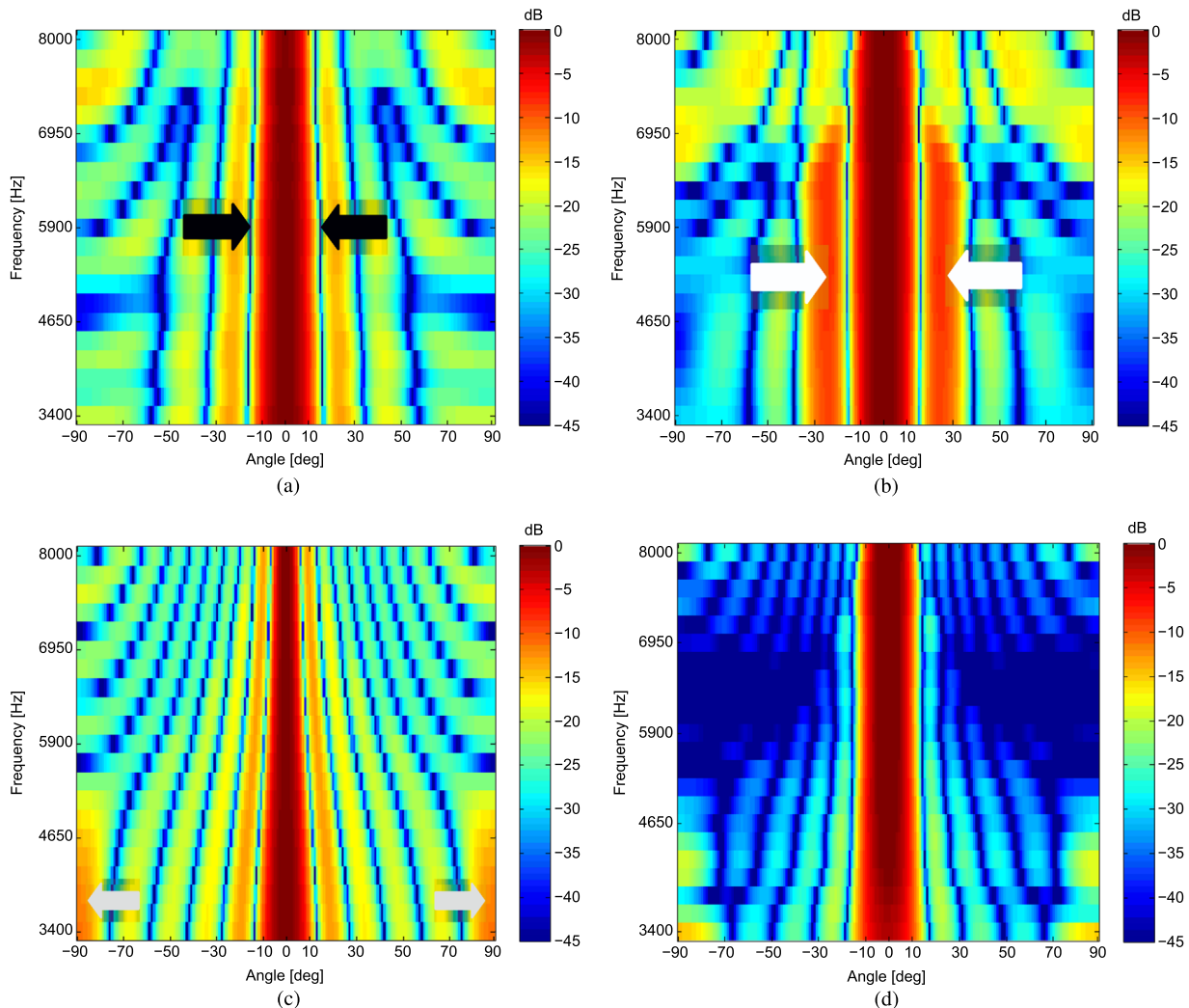


Fig. 8. Simulation results for ULA frequency response of (a) the proposed algorithm, (b) Parra's algorithm, (c) Tourbabin's algorithm, (d) Doblinger's algorithm.

different locations to have the same manifold vector (5). As a result, these sources locations cannot be uniquely determined based on the received array signals. Avoiding aliasing requires to satisfy

the condition $d < \frac{\lambda}{2}$, where λ denotes the wavelength corresponding to the angular frequency ω . On the other hand, larger d values are often used for spatial resolution improvement.

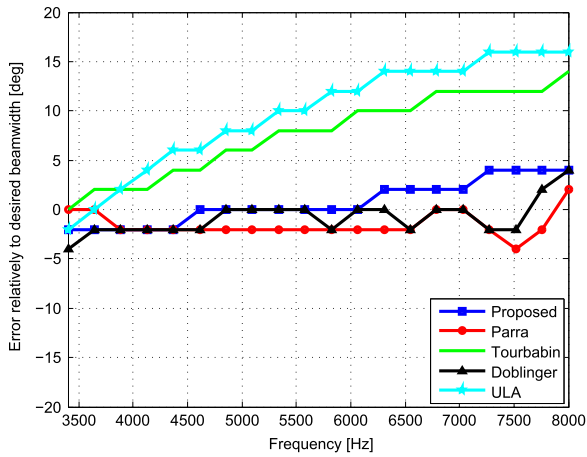


Fig. 9. Beamwidth error of the proposed algorithm (blue square), Parra's algorithm (red circle), Tourbabin's algorithm (green solid), Doblinger's algorithm (black triangle), conventional ULA (cyan star). (For interpretation of the references to color in this figure caption, the reader is referred to the web version of this paper.)

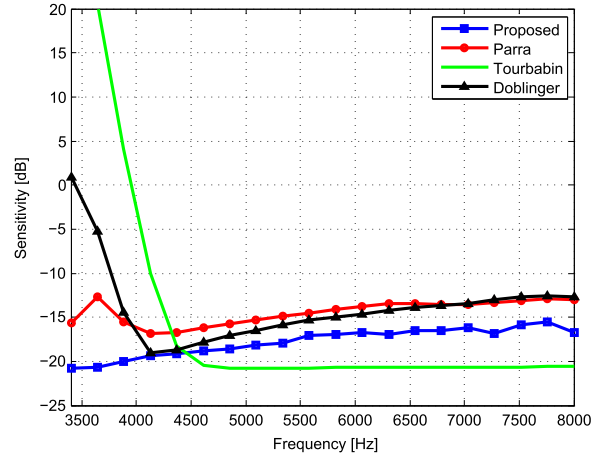


Fig. 11. Sensitivity performance of proposed algorithm (blue square), Parra's algorithm (red circle), Tourbabin's algorithm (green solid), Doblinger's algorithm (black triangle). (For interpretation of the references to color in this figure caption, the reader is referred to the web version of this paper.)

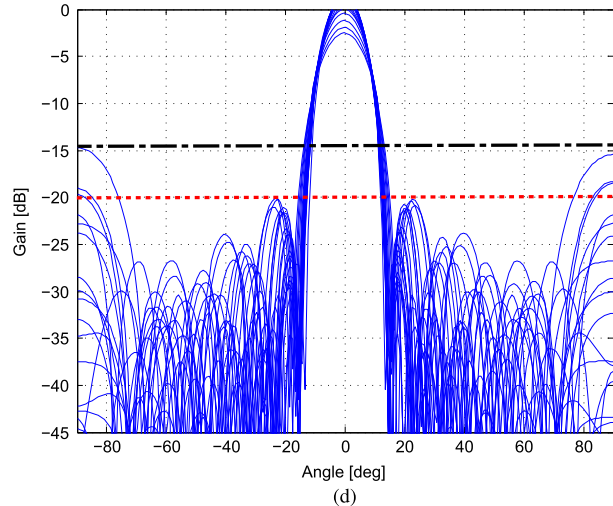
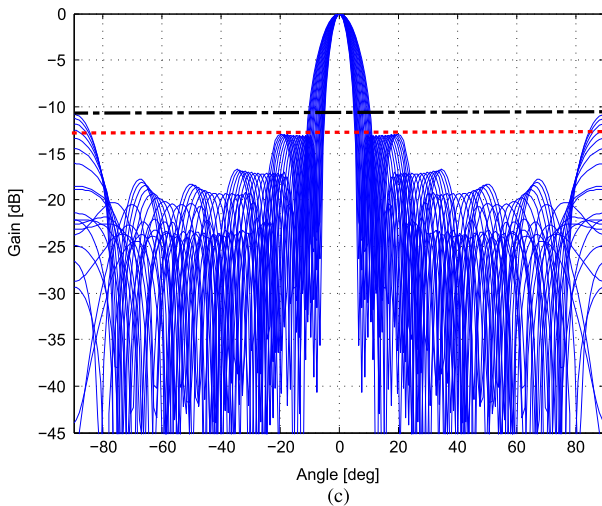
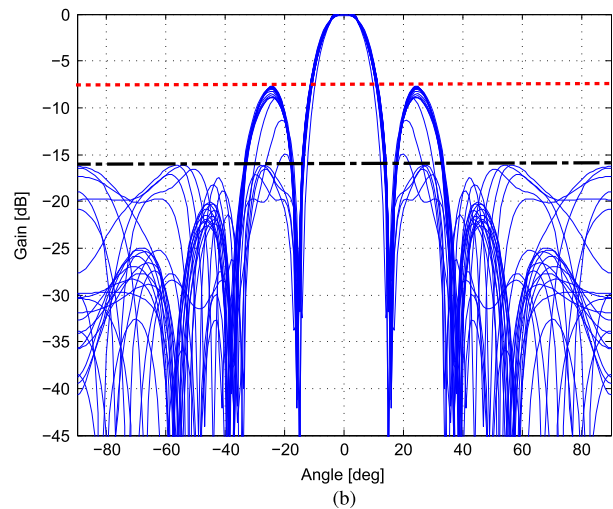
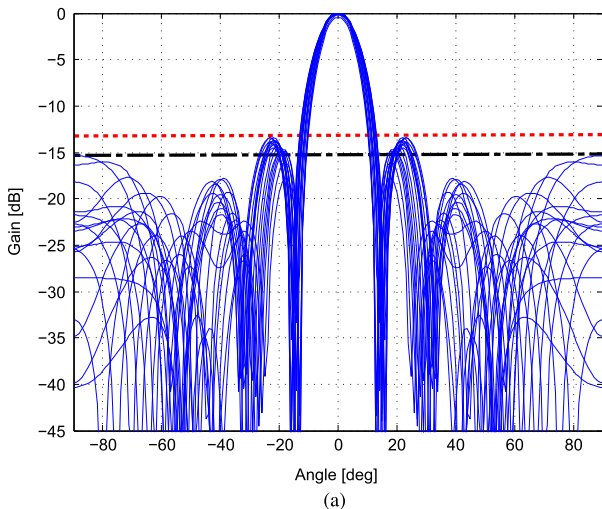


Fig. 10. Simulation results for ULA beam patterns at different frequencies of (a) the proposed algorithm, (b) Parra's algorithm, (c) Tourbabin's algorithm, (d) Doblinger's algorithm. The sidelobe levels near the main-lobe are marked by the red dashed lines and the sidelobe levels at the edges, due to aliasing, are marked by the black dash-dot lines. (For interpretation of the references to color in this figure caption, the reader is referred to the web version of this paper.)

Although spatial resolution can be improved by increasing the number of array microphones, hardware costs and array size constraints are the leading consideration in most real world applications. Aliasing is a phenomenon whose effect is stronger at higher frequencies, inducing high sidelobe levels at $\pm 90^\circ$. The proposed algorithm provides better attenuation of the high sidelobe levels at $\pm 90^\circ$, caused by aliasing, than most of the other examined methods, as seen in Fig. 10. Parra's algorithm offers slightly better aliasing attenuation because most of the energy outside of the main-lobe goes to sidelobes adjacent to the main-lobe.

4.1.4. Sensitivity

A major challenge in practical beamformer applications is the potential sensitivity to mismatches between the actual array attributes and the model used to derive the desired beamformer. In practical applications, mismatches can occur either by array spacings perturbations, production faults or filter perturbations. The sensitivity function often used as a criterion for assessing the affect of mismatches on the array response is defined in [32] by:

$$T_{se} = A_w^{-1} = \|\mathbf{w}\|^2, \tag{23}$$

where A_w^{-1} is the inverse expression of the white noise gain given by $A_w = \text{SNR}_{\text{out}}(k)/\text{SNR}_{\text{in}}(k)$ and \mathbf{w} is the weight vector corresponding to all of the FIR filter channels in the k -th frequency bin. Therefore, as the white noise gain increases, the sensitivity decreases and the array would be more robust to mismatch. In Fig. 11 the sensitivity as a function of frequency of the various algorithms is compared. The proposed algorithm yields better results for a small part of the frequency spectrum, (3400–4400) Hz, thanks to the decreasing number of effective microphones with frequency and the normalization FIR filter calculated in (23). At the higher part of the spectrum (4400–8000) Hz, the proposed algorithm produces inferior results only to the method proposed by Tourbabin since the latter minimizes the sensitivity for higher frequencies [33].

4.2. Microphone gain imperfections

For simulating microphone gain imperfections of a practical microphone array, we ran 10 simulations with a random microphone gain deviation of up to $\pm 15\%$ of the original gain and averaged the results. Fig. 12 compares the effective beamwidths of the various algorithms before and after the gain imperfection introduction. This is done by subtracting the beamwidth of the gain mismatched array from the beamwidth of the original array shown in Fig. 9, for every method.

Table 2 shows the sidelobe attenuation and the MAE from the desired beamwidth of the various methods before and after the microphone array gain perturbation. The proposed method yields the best results for sidelobe attenuation and aliasing effects attenuation when array gain perturbations are introduced. Moreover, the array perturbations have the smallest effect on the beamwidth of the proposed method since the mean absolute error has the smallest deviation before and after the gain perturbations.

4.3. Array spacings perturbations

Similar to the previous sub-section, we simulate a practical microphone array considering array spacings perturbations due to inaccuracies in microphone positioning. We ran 10 simulations with random spacing deviations of up to $\pm 10\%$ in inter-microphones spacing. We computed the beampattern as a function of frequency using (15), and then averaged the results. Fig. 13 compares the change in the effective beamwidths of the various algorithms,

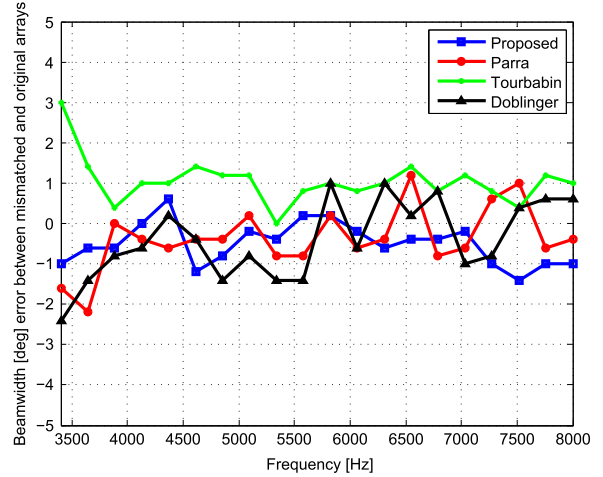


Fig. 12. Beamwidth error between the microphone gain mismatched array and original array of the proposed algorithm (blue square), Parra's algorithm (red circle), Tourbabin's algorithm (green solid) and Dobliger's algorithm (black triangle). (For interpretation of the references to color in this figure caption, the reader is referred to the web version of this paper.)

Table 2

Sidelobe attenuation of the various methods before and after the microphone array gain perturbation. The percent of degradation for every method is given in brackets.

Method	Sidelobe Atten. before/after [dB]	Sidelobe Atten. at 90° before/after [dB]	MAE before/after [deg]
Proposed	13.42/12.84 (4.32%)	15.36/14.54 (5.34%)	1.7/1.64 (3.53%)
Parra's	7.71/4.95 (35.8%)	16.42/13.96 (15%)	1.7/2.03 (19.4%)
Tourbabin's	12.92/11.09 (14.2%)	10.78/8.43 (21%)	7.7/8.76 (13.8%)
Dobliger's	20.14/16.48 (18.1%)	14.72/15.86 (7.7%)	1.4/2.11 (50%)

before and after introducing the array spacings perturbations. This is done by subtracting the beamwidth of the spacing mismatched array from the beamwidth of the original array shown in Fig. 9, for every method. It is seen that the array spacings perturbations have very little effect on the effective beamwidth of the proposed method, compared to the other examined methods, as also seen by the MAE values in the left column of Table 3.

The scenarios of array spacings perturbations and microphone gain imperfection were examined in [34]. Although an optimal solution has been successfully obtained via a min-max criterion, the solution runtime is relatively long and suitable mainly for small arrays.

Table 3 also shows the sidelobe levels of the various methods before and after the microphone array spacings perturbations. The proposed method is seen to yield the best results for sidelobe and aliasing attenuation, when array spacings perturbations are introduced.

4.4. Experimental results conclusions

Although the proposed method achieved inferior results to some methods in terms of the MAE in beamwidth, in some part of the frequency band, Fig. 10 shows that the proposed method yields better sidelobe and aliasing attenuation. The proposed method provides also a better performance, in terms of the sensitivity criterion, than the other examined algorithms in the lower part of the spectrum, as shown in Fig. 11. Finally, according to Figs. 12, 13 and Tables 2, 3, when microphone gain and positioning imperfections were introduced, the proposed method provided the most robust results in beamwidth error, having the smallest change from the nominal performance.

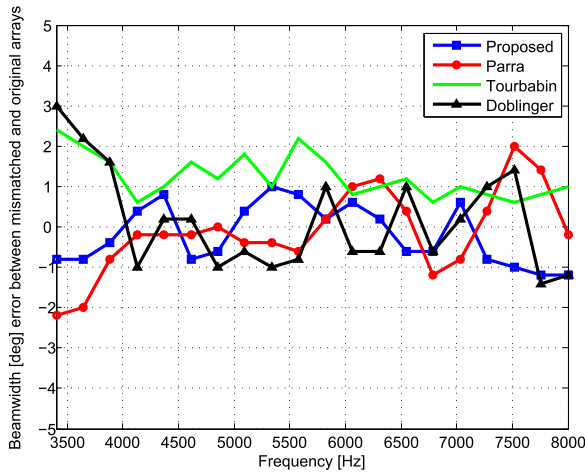


Fig. 13. Beamwidth error between the microphone spacing mismatched array and original array of the proposed algorithm (blue square), Parra's algorithm (red circle), Tourbabin's algorithm (green solid) and Doblinger's algorithm (black triangle). (For interpretation of the references to color in this figure caption, the reader is referred to the web version of this paper.)

Table 3

Sidelobe attenuation of the various methods before and after the microphone array spacings perturbation. The percent of degradation for every method is given in brackets.

Method	Sidelobe Atten. before/after [dB]	Sidelobe Atten. at 90° before/after [dB]	MAE before/after [deg]
Proposed	13.42/12.19 (9.17%)	15.36/13.1 (14.7%)	1.7/1.73 (1.76%)
Parra's	7.71/5.85 (24.12%)	16.42/13.54 (17.54%)	1.7/1.81 (6.47%)
Tourbabin's	12.92/9.84 (23.84%)	10.78/8.05 (25.32%)	7.7/8.94 (16.1%)
Doblinger's	20.14/11.21 (44.34%)	14.72/6.21 (57.81%)	1.4/1.03 (26.43%)

5. Conclusion

A new method for the design of an FIR-based constant beamwidth beamformer has been proposed. First, an input FIR filter array is designed to obtain a fixed main-lobe width in a wide frequency range. Then, an output FIR normalizing filter is designed to keep a fixed gain over that band. The proposed design method achieves a good approximation to a constant beamwidth output response, with better sidelobe and aliasing attenuation, as well as robustness to array mismatches, as compared to the other examined methods. When inducing random microphone gain and array spacings perturbations, the proposed algorithm produces steady beampatterns throughout the specified frequency band. The new method is based on designing the FIR filter array such that its frequency response reduces the number, of what we call, “effective microphones”, when signal frequency increases, affecting an approximate fixed beamwidth in a wide range of frequencies. Simulations of the proposed beamformer also demonstrate low computational complexity due to its simple closed form FIR filter design procedure. A possible future research direction could be the application of the proposed design method to other array geometries besides ULAs.

References

[1] J. Capon, High-resolution frequency-wavenumber spectrum analysis, *Proc. IEEE* 57 (8) (1969) 1408–1418.
 [2] D. Johnson, S. DeGraaf, Improving the resolution of bearing in passive sonar arrays by eigenvalue analysis, *IEEE Trans. Acoust. Speech Signal Process.* 30 (4) (1982) 638–647.

[3] G.C. McLaskey, S.D. Glaser, C.U. Grosse, Beamforming array techniques for acoustic emission monitoring of large concrete structures, *J. Sound Vib.* 329 (12) (2010) 2384–2394.
 [4] S. Fischer, K.U. Simmer, Beamforming microphone arrays for speech acquisition in noisy environments, *Speech Commun.* 20 (3) (1996) 215–227.
 [5] R.C. de Lamare, L. Wang, R. Fa, Adaptive reduced-rank lcmv beamforming algorithms based on joint iterative optimization of filters: design and analysis, *Signal Process.* 90 (2) (2010) 640–652.
 [6] D.B. Ward, Z. Ding, R.A. Kennedy, Broadband doa estimation using frequency invariant beamforming, *IEEE Trans. Signal Process.* 46 (5) (1998) 1463–1469.
 [7] W. Liu, S. Weiss, J.G. McWhirter, I.K. Proudler, Frequency invariant beamforming for two-dimensional and three-dimensional arrays, *Signal Process.* 87 (11) (2007) 2535–2543.
 [8] A. Khabbazi-basmenj, S. Vorobyov, A. Hassanien, Robust adaptive beamforming based on steering vector estimation with as little as possible prior information, *IEEE Trans. Signal Process.* 60 (6) (2012) 2974–2987.
 [9] M. Crocco, A. Trucco, Design of robust superdirective arrays with a tunable tradeoff between directivity and frequency-invariance, *IEEE Trans. Signal Process.* 59 (5) (2011) 2169–2181.
 [10] W. Liu, Adaptive wideband beamforming with sensor delay-lines, *Signal Process.* 89 (5) (2009) 876–882.
 [11] Y.I. Wu, K.T. Wong, X. Yuan, S.-k. Lau, S.-k. Tang, A directionally tunable but frequency-invariant beamformer on an acoustic velocity-sensor triad to enhance speech perception, *J. Acoust. Soc. Am.* 131 (2012) 3891.
 [12] W. Liu, S. Weiss, New class of broadband arrays with frequency invariant beam patterns, in: 2004 IEEE International Conference on Acoustics, Speech, and Signal Processing (ICASSP'04), vol. 2, 2004, pp. 185–188.
 [13] W. Zhu, W. Wu, Design of wide-band array with frequency invariant beam pattern by using adaptive synthesis method, in: 2011 IEEE International Conference on Image Analysis and Signal Processing (IASP), 2011, pp. 688–693.
 [14] Y. Zhao, W. Liu, R.J. Langley, Efficient design of frequency invariant beamformers with sensor delay-lines (2008) 335–339.
 [15] J. Li, P. Stoica, Z. Wang, On robust capon beamforming and diagonal loading, *IEEE Trans. Signal Process.* 51 (7) (2003) 1702–1715.
 [16] D. Feldman, L. Griffiths, A projection approach for robust adaptive beamforming, *IEEE Trans. Signal Process.* 42 (4) (1994) 867–876.
 [17] O. Hoshuyama, A. Sugiyama, A. Hirano, A robust adaptive beamformer for microphone arrays with a blocking matrix using constrained adaptive filters, *IEEE Trans. Signal Process.* 47 (10) (1999) 2677–2684.
 [18] R.G. Lorenz, S.P. Boyd, Robust minimum variance beamforming, *IEEE Trans. Signal Process.* 53 (5) (2005) 1684–1696.
 [19] Y. Bucris, I. Cohen, M. Doron, Bayesian focusing for coherent wideband beamforming, *IEEE Trans. Audio Speech Lang. Process.* 20 (4) (2012) 1282–1296.
 [20] G. Doblinger, Optimization of wideband fixed beamformers with adaptive sensor calibration, in: 18th European Signal Processing Conference, 2010, pp. 2062–2066.
 [21] T. Yardibi, J. Li, P. Stoica, M. Xue, A.B. Baggeroer, Source localization and sensing: a nonparametric iterative adaptive approach based on weighted least squares, *IEEE Trans. Aerosp. Electron. Syst.* 46 (1) (2010) 425–443.
 [22] Y. Zhao, W. Liu, R. Langley, A least squares approach to the design of frequency invariant beamformers, in: Proceedings of European Signal Processing Conference, Glasgow, Scotland, 2009, pp. 844–848.
 [23] K. Slavakis, I. Yamada, Robust wideband beamforming by the hybrid steepest descent method, *IEEE Trans. Signal Process.* 55 (9) (2007) 4511–4522.
 [24] S. Markovich, S. Gannot, I. Cohen, Multichannel eigenspace beamforming in a reverberant noisy environment with multiple interfering speech signals, *IEEE Trans. Audio Speech Lang. Process.* 17 (6) (2009) 1071–1086.
 [25] S. Yan, Y. Ma, Design of fir beamformer with frequency invariant patterns via jointly optimizing spatial and frequency responses, in: 2005 IEEE International Conference on Acoustics, Speech, and Signal Processing (ICASSP'05), vol. 4, 2005, pp. 789–792.
 [26] L.C. Parra, Steerable frequency-invariant beamforming for arbitrary arrays, *J. Acoust. Soc. Am.* 119 (2006) 3839.
 [27] S. Yan, Optimal design of fir beamformer with frequency invariant patterns, *Appl. Acoust.* 67 (6) (2006) 511–528.
 [28] S. Yan, H. Sun, X. Ma, U. Svensson, C. Hou, Time-domain implementation of broadband beamformer in spherical harmonics domain, *IEEE Trans. Audio Speech Lang. Process.* 19 (5) (2011) 1221–1230.
 [29] S. Doclo, M. Moonen, Design of far-field and near-field broadband beamformers using eigenfilters, *Signal Process.* 83 (12) (2003) 2641–2673.
 [30] W. Liu, S. Weiss, *Wideband Beamforming: Concepts and Techniques*, John Wiley & Sons, Chichester, UK, 2010.
 [31] D.B. Ward, R.A. Kennedy, R.C. Williamson, Fir filter design for frequency invariant beamformers, *IEEE Signal Process. Lett.* 3 (3) (1996) 69–71.
 [32] H.L. Van Trees, *Detection, Estimation, and Modulation Theory, Optimum Array Processing*, John Wiley & Sons, New-York, USA, 2004.
 [33] V. Tourbabin, M. Agmon, B. Rafaely, J. Tabrikian, Optimal real-weighted beamforming with application to linear and spherical arrays, *IEEE Trans. Audio Speech Lang. Process.* 20 (9) (2012) 2575–2585.
 [34] S. Doclo, M. Moonen, Design of broadband beamformers robust against gain and phase errors in the microphone array characteristics, *IEEE Trans. Signal Process.* 51 (10) (2003) 2511–2526.